Proton scattering on $A=92-116$ nuclei with extended optical models and the interacting boson approximation

E. Cereda, M. Pignanelli, and S. Micheletti
Istituto di Fisica dell'Università di Milano, Milano, Italy
and Istituto Nazionale di Fisica Nucleare, Sezione di Milano, Milano, Italy

H. V. von Geramb
Universität Hamburg, D-2000 Hamburg 50, West Germany

M. N. Harakeh
Kernfysisch Versneller Instituut, Rijksuniversiteit Groningen, The Netherlands

R. De Leo, G. D'Erasmo, and A. Pantaleo
Istituto di Fisica dell'Università di Bari, Bari, Italy
and Istituto Nazionale di Fisica Nucleare, Sezione di Bari, Bari, Italy
(Received 21 July 1982)

Differential cross sections for proton elastic and inelastic scattering have been measured at $E_p=22.3$ MeV for 14 nuclei with $92\leq A\leq 116$. The energy dependence has been studied between 10 and 35 MeV, considering also reaction cross sections at lower incident energies. The long standing sub-Coulomb optical model anomalies are thereby eliminated. Nuclear structure effects found in the analysis of elastic scattering are identified with strong couplings between ground and one-phonon states. These couplings are satisfactorily described by traditional collective models, using deformation parameters in agreement with those deduced from electromagnetic data. The transitions to weakly excited states require a more accurate spectroscopic description. Spectroscopic amplitudes taken from the interacting boson model are used. The radial dependence of transition densities is derived from optical model potentials.

NUCLEAR REACTIONS Proton scattering on ^{92,94,96,98,100}Mo, ^{102}Ru, ^{104,106,108,110}Pd, and ^{106,110,112,116}Cd; $E_p=22.3$ MeV; on ^{104}Pd at $E_p=10.25$, 12.1, 15.0, 17.3, 22.3, 30.2, and 35.4 MeV. Measured $\sigma(\theta)$; enriched targets. Optical model and coupled channels analyses. Collective vibrational model, coupling parameters. Interacting bosons approximation, form factors.

I. INTRODUCTION

The properties of the low-lying excited states of even-even nuclei in the $A=90-120$ mass region have been extensively studied for more than a decade with Coulomb excitation and electron or nucleon scattering. In the present measurements new and more complete data on the energy and mass dependence of proton scattering in the region of mass-100 nuclei have been taken. These are used to obtain a better understanding of some aspects of this nuclear mass region which have been of interest for some time, but are still not completely understood.

The first concerns the behavior of the optical model (OM) potentials. The anomalous increase of the absorptive part of the OM potentials found by Johnson *et al.*[1] at sub-Coulomb incident energies for the region of $A=100-110$ is puzzling. In fact, systematic studies of OM parameters, as well as of microscopic OM potentials, show generally only small variations due to shell effects and a smooth behavior in energy and mass.

A second problem is connected with coupled channels (CC) calculations based on the vibrational model of the nucleus.[2-7] It has been known for

some time that agreement with the experimental differential cross sections can be reached only using various methods, i.e., alterations in the values of OM parameters or of coupling strengths, but these methods do not always lead to reliable results. For instance, most of the CC analyses of (p,p') experiments on Pd and Cd isotopes gave coupling strengths, for certain transitions, systematically in disagreement with $B(E2)$ values.[4] A recent solution of this second problem was offered by the interacting boson approximation (IBA).[8–10] Of particular interest for the present study is the recent use of the IBA model to extract transition form factors from electron scattering data.[11] We apply the IBA model to describe inelastic proton scattering from several Mo, Pd, and Cd isotopes, using deformed optical potentials in CC calculations which include the relevant spectroscopic amplitudes obtained from the IBA. The proton scattering data are therefore analyzed with a minimum number of adjustable parameters, so as to reduce the uncertainties notoriously associated with many-parameter searches.

In the next section the salient features of the experiment are described. The mass dependence of proton scattering has been studied at 22.3 MeV, using the nuclei ^{92,94,96,98,100}Mo, ^{102}Ru, ^{104,106,108,110}Pd, and ^{106,110,112,116}Cd. The energy dependence has been studied between 10 and 35 MeV for ^{104}Pd. Section III describes the analysis of the energy dependence and in particular of the sub-Coulomb data. In Sec. IV we present the analysis of elastic and inelastic scatterings performed with CC calculations, based on the vibrational model.[12] This traditional picture of the nucleus has been used to clarify the correlations between OM parameters and coupling schemes. Finally, Sec. V contains the results of CC calculations based on IBA spectroscopic amplitudes.

II. EXPERIMENTAL METHOD

The protons, accelerated by the AVF Milan cyclotron, were momentum analyzed by a 120°-bending magnet and focused to a spot of 3–4 mm in diameter at the center of a 60-cm diameter scattering chamber.

The isotopic enrichment of the target nuclei was generally between 96 and 98% except for ^{106}Cd (90.8%) and ^{106}Pd (75.5%). The areal density of the targets was estimated by weighing and measuring the energy loss of alpha particles emitted by an ^{241}Am source. The latter method, when properly used, allows precise relative measurements and avoids the effects resulting from the nonuniformity of the foils. The estimated uncertainty in target thickness is of the order of 5–7% and of the absolute cross sections of less than 10%. These values must be considered as conservative estimates. In fact, the factors needed to normalize the theoretical predictions, obtained with average OM parameters, to the measured elastic scattering cross sections, differ from unity by no more than 2–3%.

Three surface barrier silicon detectors, 3000 μm thick, were used to observe the scattered protons. Telescopes made by 2000 and 5000 μm detectors

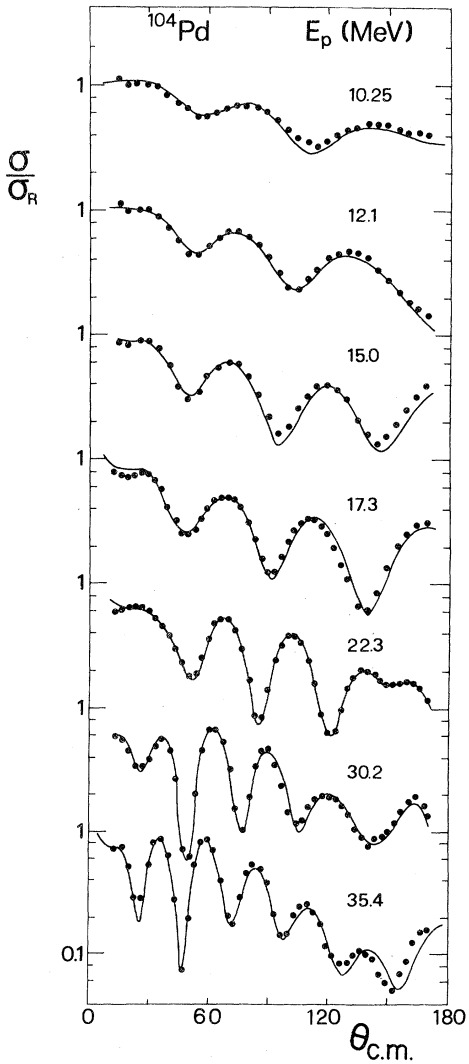

FIG. 1. Differential cross sections for proton elastic scattering on ^{104}Pd at different incident energies. The solid curves are the results of coupled channels calculations with the coupling scheme $(0_0^+\text{-}2_1^+\text{-}3_1^-)$ and the parameters of Table I.

were used for incident energies higher than 23 MeV. The overall energy resolution of the present experiment was of the order of 40 keV.

The proton angular distributions were measured in steps of 3.3° from 13.3° to 170° laboratory angles. The transition to the ground state and the 2_1^+ and 3_1^- states were measured for all targets and incident energies; data have been also collected for the triplet of states 0^+, 2^+, and 4^+ (the second 0^+ and 2^+ and the first 4^+ excited states). The quality of the latter data is more affected by the limited energy resolution and by scattering from carbon and oxygen contaminants in the targets.

III. ENERGY DEPENDENCE, RESULTS, AND ANALYSIS

A. ^{104}Pd data

The isotope ^{104}Pd has been chosen for this study of the energy dependence of proton scattering because of its position at the center of the A region in which large anomalies in the OM parameters had been deduced.[1] Figures 1–3 show the experimental differential cross sections, measured at seven different incident energies between 10.25 and 35.4 MeV.

Both OM and CC analyses were performed with the automatic search code ECIS.[13] The OM poten-

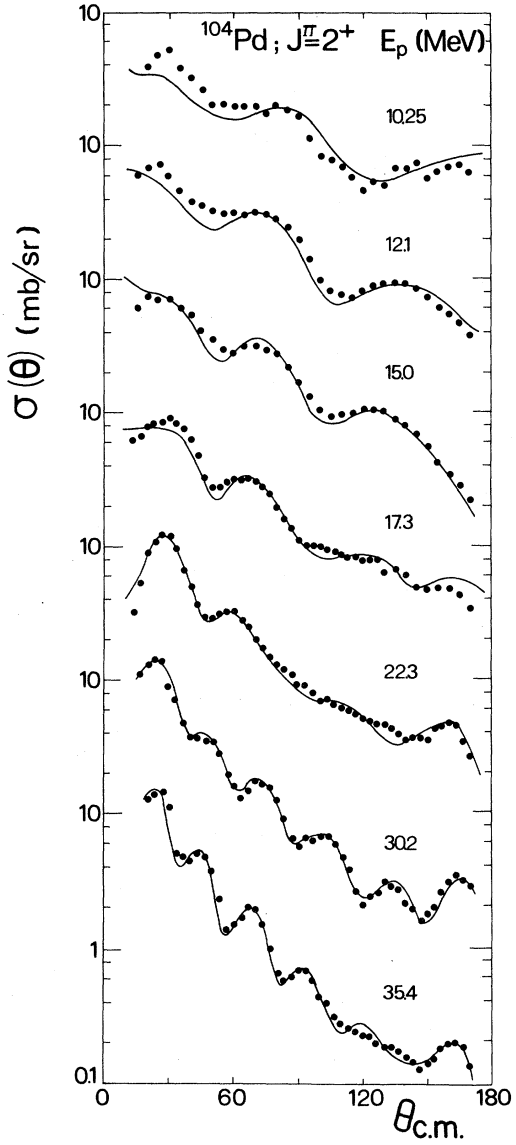

FIG. 2. Differential cross sections for proton inelastic scattering to the 2_1^+ state of ^{104}Pd; see Fig. 1 caption.

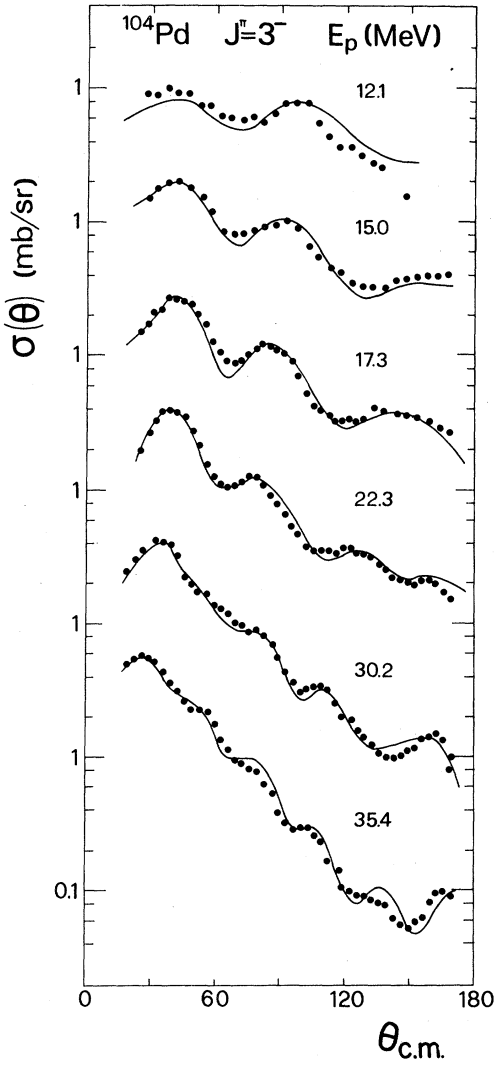

FIG. 3. Differential cross sections for proton inelastic scattering to the 3_1^- state of ^{104}Pd; see Fig. 1 caption.

TABLE I. Least-square values of the optical model parameters for ^{104}Pd from coupled channels calculations assuming a first-order vibrational model and the $(0_0^+\text{-}2_0^+\text{-}3_1^-)$ coupling scheme. The other parameters were fixed at the following energy-independent values: $r_0=1.165$, $a_0=0.781$, $r_w=1.276$, $a_w=0.698$, $V_{so}=6$, $r_{so}=1.01$, $a_{so}=0.75$, and $r_C=1.2$. The well depths are in MeV and the geometrical parameters in fm. $RW2$ and $RW3$ give, respectively, the ratio of the volume integral of the 2_1^+ and 3_1^- imaginary potentials to that for the elastic channel.

E_{inc} (MeV)	V_0 (MeV)	W (MeV)	W(g.s.) (MeV)	$W_D(2^+)$ (MeV)	$W_D(3^-)$ (MeV)	$RW2$	$RW3$	β_2	β_3
10.2	58.0		7.15	7.15		1.00		0.1751	
12.1	57.9		7.77	7.88	7.56	1.01	0.97	0.2055	0.1802
15.0	56.4		7.43	10.18	7.12	1.37	0.96	0.2248	0.1756
17.3	56.1		8.18	9.44	8.86	1.16	1.08	0.2000	0.1813
22.3	54.0	0.50	7.87	11.61	8.06	1.45	1.03	0.2342	0.1706
30.2	51.1	3.43	5.20	6.03	4.96	1.11	0.97	0.2064	0.1561
35.4	48.2	5.36	3.42	4.38	4.10	1.13	1.09	0.2187	0.1760

tial used was of the form

$$U(r)= V_C(r)-V_0 f(r,R_0,a_0)-iWf(r,R_w,a_w)$$
$$+4ia_w W_D \frac{d}{dr} f(r,R_w,a_w)$$
$$+(\hbar/M_\pi c)^2 \frac{V_{so}}{r}\frac{d}{dr} f(r,R_{so},a_{so})\bar{\sigma}\cdot\bar{L} ,$$

where

$$f(r,R_i,a_i)=\{1+\exp[(r-R_i)/a_i]\}^{-1} ;$$

$R_i=r_i A^{1/3}$, and $V_C(r)$ is the Coulomb term. Initially all the parameters were searched on in a best-fit procedure, considering only the elastic scattering data. After this preliminary search the spin-orbit and geometrical parameters of the real central term were fixed at energy-independent values. The inelastic angular distributions were then taken into account in CC calculations assuming collective vibrations, and considering only first-order coupling terms. The well depths for the central terms (real and imaginary) and the deformation parameters β_2 and β_3 were searched on, with a different absorption allowed for each channel. The values of W_D for the 3^- state were practically equal to those for the elastic channel, as shown by the ratios $RW3$ in Table I. Larger W_D values were instead required by the 2_1^+ channel for incident energies higher than 15 MeV. The values of β_λ fluctuate around the electromagnetic values,[14–22] which are given in Table II also for the other nuclei concerned. No evidence for any anomaly or special feature has been found except that a larger W_D value is required for the 2_1^+ channel. Data at lower incident energies, such as those for 6 MeV proton scattering from Pd isotopes by Antropov *et al.*,[23] can be reproduced using the geometries given in Table I and standard well depths. As it had already been shown by the above authors,[23] data taken at an incident energy slightly below the Coulomb barrier can therefore be reproduced by standard OM parameters.

B. Sub-Coulomb data

In a recent study of the (p,n) reaction on $89 \leq A \leq 130$ nuclei, Johnson, Galonsky, and Ker-

TABLE II. Values of quadrupole and octupole deformation parameters from electromagnetic data (Refs. 15–22) assuming a uniform charge-density distribution with a radius $R_C=1.2\,A^{1/3}$.

Nucleus	β_2	β_3	Nucleus	β_2	β_3
^{92}Mo	0.1085	0.158	^{106}Pd	0.2290	0.170
^{94}Mo	0.1522	0.153	^{108}Pd	0.2430	0.149
^{96}Mo	0.1716	0.182	^{110}Pd	0.2580	0.140
^{98}Mo	0.1740	0.220	^{106}Cd	0.1709	0.170
^{100}Mo	0.2298	0.210	^{110}Cd	0.1737	0.147
^{102}Ru	0.2460	0.149	^{112}Cd	0.1814	0.147
^{104}Pd	0.2090	0.170	^{116}Cd	0.1860	0.131

nell[1] obtained evidence for a strong A dependence of OM potentials at sub-Coulomb proton energies. At these energies the (p,n) channel represents a large fraction of the total reaction cross section σ_R and should therefore be very significant in determining the imaginary part of the OM potential. The anomalously large values of the imaginary well depth, which these authors found around $A=105$, are the most striking aspect of this A dependence.

The OM analysis of Johnson *et al.*[1] is certainly a very simple parametrization of a large amount of data. The excitation functions for 19 nuclei are in fact reproduced by OM potentials with most of the parameters practically fixed at standard values. Only W_D was really used as a free parameter and was varied with A, between 5 MeV (^{89}Y) and 97 MeV (^{103}Rh), but not with incident energy. At very low incident energies the cross sections are determined mainly by the transmission factors and by their sensitivity to the geometries of the potentials. For this reason the neglect of even a small variation in a well radius, required by the structure of the nucleus, cannot be compensated for by a small adjustment of W_D. Electric charge data indicate that shell effects can account for variations of the rms radii of the order of a few percent.[24] Figure 4 shows the dependence of σ_R on W_D for ^{103}Rh, obtained by using the OM potential of Ref. 1 (full lines) and that (dashed lines) calculated with small and acceptable variations of some parameters: V_0, from $(62.7-0.32E)$ to $(64-0.55E)$ MeV, r_0, from 1.2 to 1.17 fm, and a_W, from 0.39 to 0.5 fm. The energy dependence of V_0 at very low incident energies is not well known, but it is commonly accepted that it could be larger than at higher incident energies. As is also shown in Ref. 1 [Fig. 19(c)], a strong dependence in the real well depth can improve the agreement with the experimental excitation functions. With these variations a standard imaginary well of about 8 MeV gives σ_R in reasonable agreement with the experiment. From the same figure it is also evident that the use of a very deep imaginary potential gives rise to a saturation

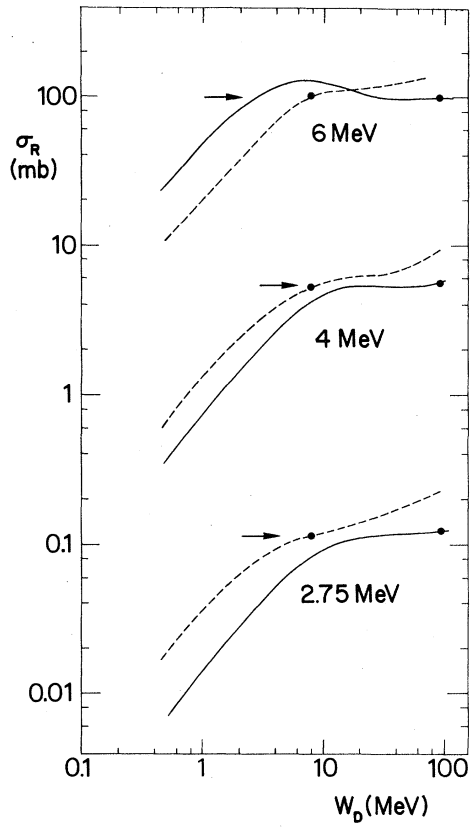

FIG. 4. Calculated total reaction cross sections for proton scattering on ^{103}Rh, plotted against the imaginary well depth, at three incident energies. The solid curves are from the OM potentials of Ref. 1. The dashed curves were obtained with small adjustments in some parameters (see text). The points give the W_D values with which the calculations reproduce the experimental cross sections (arrows).

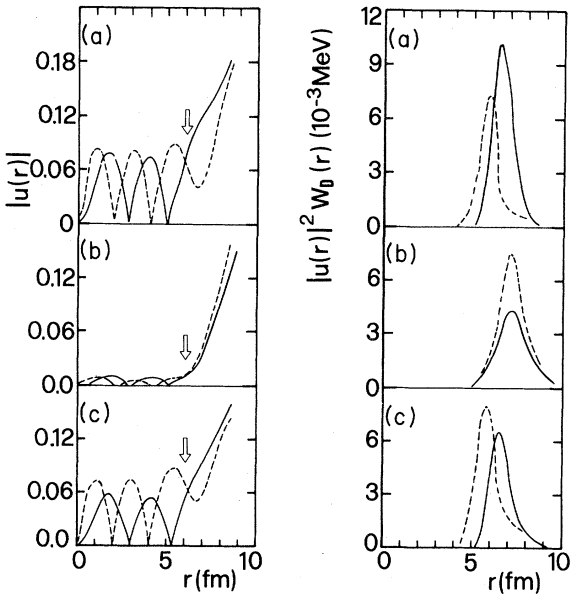

FIG. 5. Optical model calculations for 5 MeV proton scattering on ^{103}Rh. On the left side: absolute values of the s (dashed curves) and p wave functions (solid curves) obtained with three different potentials (see text), which all reproduce the experimental total reaction cross section. The vertical arrows mark the location of the maximum of the three imaginary wells. The right side shows the corresponding distribution of the absorption probability.

in σ_R which makes it no longer W_D dependent. It is then easier to fit the data over the full energy range with a constant W_D value. On the other hand, considering the effects of the Pauli principle, the use of an energy-independent imaginary potential can hardly be justified. The energy dependence of $W_D(r)$ should therefore be considered. However, the crucial point is certainly that of the role of a dimension resonance for the $3p$ wave.[1,25] At incident energies of about 5 MeV, using the OM parameters of Ref. 1 with a "normal" W_D (<12 MeV), one finds that, for $A \sim 100$, the contribution coming from the p wave becomes larger than that of the s wave [Fig. 5(a)]. A large p wave contribution is not required by the experiment up to $A \sim 112$. Since the absorption, and therefore σ_R, are proportional to $|u(r)|^2 W_D(r)$, it is possible[1] to damp out this unwanted resonance by reducing the amplitude of the wave function $u(r)$ by using a very large W_D [Fig. 5(b)]. An equivalent result [Fig. 5(c)] can also be obtained with the same small adjustments of some OM parameters used for the dashed curves of Fig. 4.

Finally, one should note that the anomaly in the A dependence found for W_D is, in a certain sense, only apparent. To show this, we can consider the $W_D(r)$ wells, which had been used[1] for ^{93}Nb, ^{103}Rh, and ^{110}Pd. These wells have an integrated volume of 49, 695, and 117 MeV fm^3, respectively. But the incoming proton is not sensitive to the same extent to the inner part of the $W_D(r)$ well, as can be shown

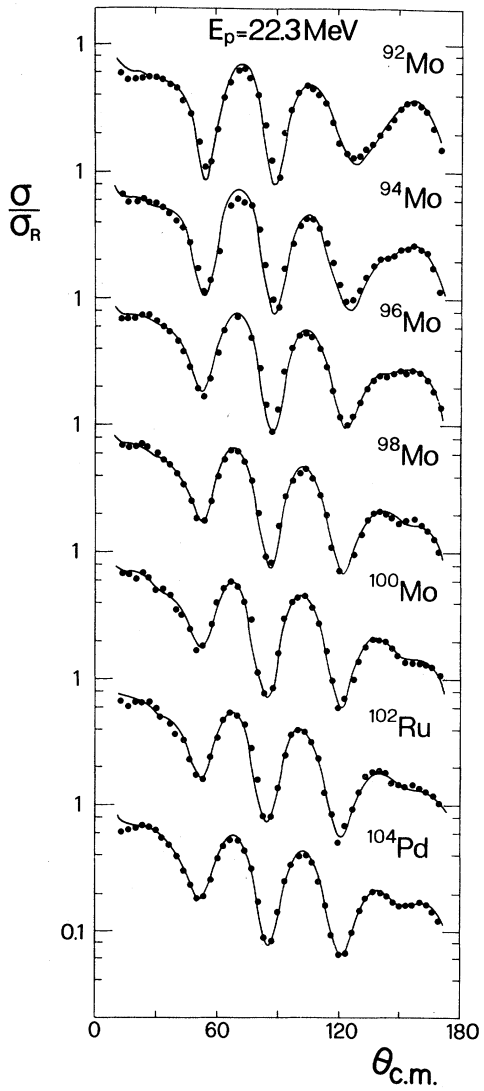

FIG. 6. Differential cross sections for proton elastic scattering at 22.3 MeV on even-even nuclei $92 \leq A \leq 104$. The curves are from optical model calculations performed with the parameters of Table III.

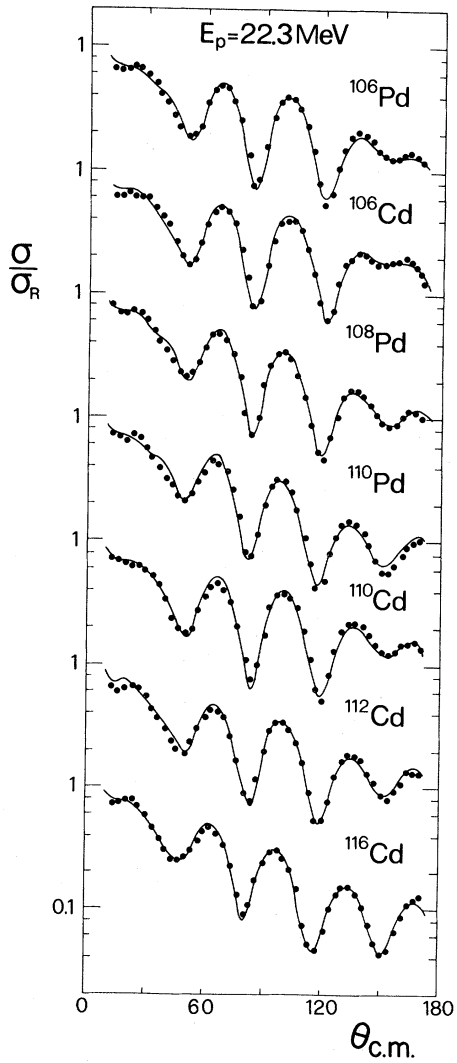

FIG. 7. Same as in Fig. 6, for $106 \leq A \leq 116$.

by introducing a lower cutoff. Eighty percent of σ_R is obtained from the contributions at radial distances larger than 5.8, 7.5, and 7.1 fm, with volume integrals of 30, 28.5, and 32 MeV fm^3, respectively. The effective imaginary potentials are therefore not substantially different for the three nuclei cited above.

Concluding this section, it has been shown that a reanalysis of the data of Johnson *et al.*,[1] with more flexibility in the search of the parameters, could reduce the anomaly found in the single-parameter analysis. In this reanalysis, in order to avoid possible ambiguities, the (p,n) cross sections should be supplemented by other data, such as precise elastic scattering cross sections.[25] No evidence, in any case, has been found for anomalies at incident proton energies above the Coulomb barrier.

IV. MASS DEPENDENCE

A. One-phonon states and the harmonic vibrator model

The elastic scattering data collected at 22.3 MeV have been first compared with OM predictions (Figs. 6 and 7). The resulting OM parameters are given in Table III. The volume integrals J_V and J_W of the real and the imaginary central terms are plotted in Figs. 8 and 9 against the asymmetry $(N-Z)/A$. The J_W values are rather large but they follow the usual expectations,[26] while the trend of J_V is significantly inconsistent with the prediction of the Lane model, especially for Cd and Pd isotopes. This behavior had been studied by Comfort[27] for Mo isotopes and interpreted in terms of shell effects by introducing the coupling of the elastic channel to the relevant (p,d) channels. These couplings have been considered also in the present analysis, but without satisfactory results. As will become clear below, the magnitude of J_W and the anomalous J_V isospin dependence can be understood by considering the relevant inelastic channels. Their effect has been taken into account using CC calculations. Different assumptions have been adopted in an effort to understand the connection between coupling schemes, coupling strengths, and OM parameters. These are summarized in Table IV. The χ^2 values and other quantities (defined below), averaged over the nuclei from ^{94}Mo to ^{116}Cd, are also given. The results for ^{92}Mo will be discussed separately. The excitation of the first quadrupole and octupole state of each isotope has been calculated using a $(0_0^+\text{-}2_1^+\text{-}3_1^-)$ coupling scheme, where the subscripts indicate the number of

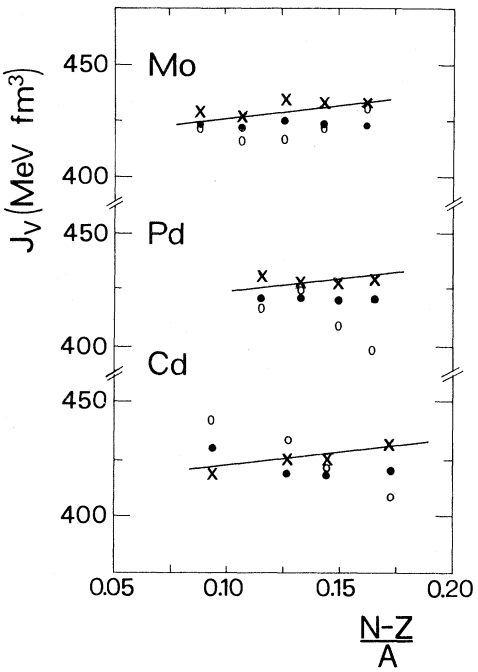

FIG. 8. Asymmetry dependence of the volume integral per nucleon of the central real part of the OM potentials used in optical model calculations (empty points), coupled channels calculations with first-order vibrational model and coupling scheme $(0_0^+\text{-}2_1^+\text{-}3_1^-)$ (crosses), and second-order vibrational model with the coupling scheme $(0_0^+\text{-}2_1^+\text{-}0_2^+\text{-}2_2^+\text{-}4_2^+)$ (full points). The solid lines give the asymmetry dependence of Becchetti-Greenlees proton potentials (Ref. 26).

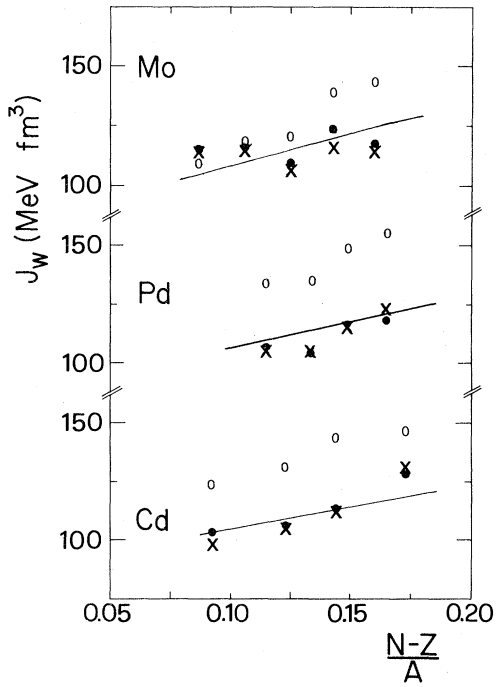

FIG. 9. Same as in Fig. 8 for the imaginary terms.

TABLE III. Optical model parameters used in the analysis of 22.3 MeV elastic scattering data. The parameters not reported in the table have been taken for all the nuclei as $W=0.5$, $V_{so}=6$ MeV; $r_w=1.276$, $r_{so}1.01$, $r_c=1.2$, $a_{so}=0.75$ fm. The χ^2 values, given in the last column, are per point and have been calculated assuming a constant experimental error of 10%.

Nucleus	V_0 (MeV)	r_0 (fm)	a_0 (fm)	W_D (MeV)	a_w (fm)	χ^2
^{92}Mo	52.5	1.165	0.810	8.32	0.694	1.37
^{94}Mo	51.9	1.169	0.780	9.11	0.687	1.00
^{96}Mo	52.4	1.182	0.685	9.63	0.666	0.23
^{98}Mo	52.7	1.173	0.755	10.9	0.67	0.32
^{100}Mo	53.4	1.165	0.810	12.0	0.640	0.42
^{102}Ru	52.6	1.165	0.792	10.7	0.685	0.52
^{104}Pd	52.8	1.170	0.738	10.3	0.692	0.42
^{106}Pd	52.8	1.165	0.811	11.1	0.649	0.44
^{108}Pd	54.1	1.143	0.783	10.1	0.771	0.60
^{110}Pd	52.3	1.149	0.760	9.51	0.848	0.69
^{106}Cd	53.2	1.182	0.797	11.0	0.600	0.58
^{110}Cd	52.5	1.174	0.816	11.0	0.630	0.65
^{112}Cd	54.3	1.145	0.827	10.9	0.702	0.95
^{116}Cd	53.1	1.166	0.700	8.50	0.890	0.67

vibrational phonons. If average geometrical parameters are used instead of the best-fit values of Table III, the quality of the fits of the 2_1^+ data is greatly improved at the cost of a very limited worsening of those to the elastic scattering. The well depths and deformabilities deduced with average geometries are listed in Table V. The calculated curves for the 2_1^+ transitions oscillate more than the experimental data in the angular region between 70° and 130° (dashed curves in Figs. 10 and 11).

These oscillations can be smeared out by introducing second-order terms. The solid curves given in Figs. 10 and 11 are the results of a second-order vibrator calculation, carried out to explore the effect of the inclusion of the triplet of two-quadrupole-phonon states, that is to say assuming the scheme (0_0^+-2_1^+-0_2^+-2_2^+-4_2^+). It must be noted that, using this notation for phonon numbers, the first 4^+ state is indicated as 4_2^+ in the hypothesis of a dominant two-phonon structure. In this calculation the levels of the triplet are simply considered as pure two-phonon states, without requiring good fits. The agreement with 2_1^+ differential cross sections and with electromagnetic quadrupole parameters is good, and the deduced OM parameters (Table VI) are free from relevant nuclear structure effects. These satisfactory results indicate that in spite of the naive picture used for the structure of the 0_2^+, 2_2^+, and 4_2^+ states, most of the collective couplings required by the 2_1^+ channel are taken into account. In contrast the same calculation causes a worsening (by a factor of 2 in the χ^2) of the fits to the elastic scattering. This is due to a too large effect of the second-order terms. The same is probably true also for the 2_1^+ transitions. In this case, however, they can be overestimated if the reorientation terms (transitions between magnetic substates of the same state in a deformed nucleus) are not taken into account, as in the vibrational model. In the case of the nuclei studied here, the relatively large values of the intrinsic quadrupole moments Q_{2+} of the 2_1^+ states[17,19,22] indicate that these reorientation terms should be included.

The fits of the 3_1^- data, shown in the Figs. 12 and 13, are less satisfactory and cannot be easily improved. The second-order terms are not in fact very helpful and the possible couplings with other states cannot be introduced owing to the lack of relevant information. The ratios of deformation parameters $\beta^{pp'}$ from the present analysis, to their electromagnetic values β^{em}, deduced from $B(E2)$ values assuming, as usually, a uniform charge density distribution with a radius $R_C=1.2\ A^{1/3}$ (see Table II), are given as $R\beta 2$ and $R\beta 3$ in Table IV. In the same table the quantities $RW2$ and $RW3$ give, respectively, the average ratios of the volume integral of the imaginary potential W_D needed by the 2_1^+ and 3_1^- channels to that of the elastic channel. $RW0$ is the ratio of the imaginary potentials used in CC and OM calculations. The values of RW0 show that the reduction in W_D is mainly determined by the coupling with the 2_1^+ channel and is of the order of 15%. This reduction is less marked than that found in the case of rotational nuclei.[28] The ima-

TABLE IV. Summary of the collective model calculations. In the second column the symbols HVM, 1st Or, 2nd Or, and RT stand, respectively, for harmonic vibrational model, first- and second-order calculations, and reorientation terms. The numbers given in columns 3–11 are the values of different quantities averaged from ^{94}Mo to ^{116}Cd. The χ^2s are defined as in Table III; $RW2$ and $RW3$ as in Table I. $RW0$ is the ratio of the imaginary potential for the elastic channel used in coupled-channel calculations to that used in optical model calculations. $R\beta_2$ and $R\beta_3$ give the ratios of $\beta_\chi^{pp'}$ (present analyses) to β_χ^{em} (see Table II).

OM potential	Model	Coupling scheme	χ^2/N (g.s.)	χ^2/N 2^+	χ^2/N 3^-	$R\beta_2$	$RW2$	$R\beta_3$	$RW3$	$RW0$
Best fit[a]	OM	0_0^+	0.57							1
Best fit[a]	HVM, 1st Or	0_0^+-2_1^+-3_1^-	0.65	2.37	2.09	1.11±0.11	1.41	1.01±0.10	1.09	0.83
Average[b]	HVM, 1st Or	0_0^+-2_1^+-3_1^-	0.74	1.21	2.22	1.10±0.05	1.37	0.99±0.04	1.05	0.84
Average[b]	HVM, 1st Or	0_0^+-2_1^+-3_1^-	0.76	1.46	2.13	1[c]	1.18	1[c]	1.06	0.83
Average[d]	HVM, 1st Or	0_0^+-2_1^+-3_1^-	0.82	1.89	2.18	0.91±0.03	1[d]	1.00±0.07	1[d]	0.85
Average[b]	HVM, 1st Or	0_0^+-2_1^+	0.87	1.10		1.16±0.09	1.40			0.86
Average[b]	HVM, 2nd Or	0_0^+-2_1^+	1.36	1.10		1.03±0.08	1.17			0.84
Average[b]	HVM, 1st Or, RT	0_0^+-2_1^+	1.25	0.75		1.08±0.07	1.28			0.84
Average[b]	HVM, 2nd Or	0_0^+-2_1^+-0_2^+-2_2^+-4_2^+	1.32	0.87		1.03±0.08	1.03			0.86
Average[d]	HVM, 2nd Or	0_0^+-2_1^+-0_2^+-2_2^+-4_2^+	1.31	0.94		1.01±0.03	1[d]			0.84
Average[d]	HVM, 2nd Or	0_0^+-2_1^+-3_1^--0_2^+-2_2^+-4_2^+	0.92	1.23	2.30	0.93±0.04	1[d]	0.99±0.09	1[d]	0.84

[a]See Table III.
[b]See Table V.
[c]Assuming $\beta_\chi^{pp'}=\beta_\chi^{em}$.
[d]As in b, but assuming $W_D(\text{g.s.})=W_D(2^+)=W_D(3^-)$.

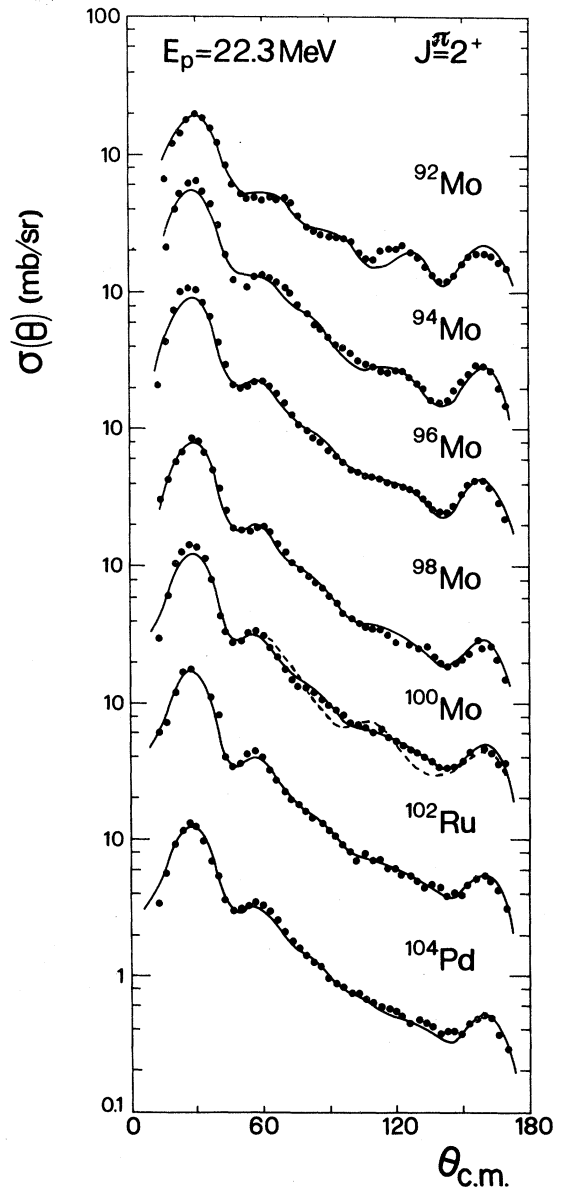

FIG. 10. Differential cross sections for the excitation of the first 2^+ state of the $92 \leq A \leq 104$ nuclei. The dashed curve for ^{100}Mo is given as an example of a first-order calculations. The solid curves are from coupled channels calculations in the framework of a second-order vibrational model with the (0_0^+-2_1^+-0_2^+-2_2^+-4_2^+) coupling scheme.

ginary term for the 2_1^+ channel (see the $RW2$ values) is approximately equal to that for the ground state when the two-phonon states are considered in a second-order calculation; when these are neglected it is larger by 15% and up to 40% in a first-order calculation. An increase of this order had already been found at lower incident energies,[2,4] and is similar to or larger than those found for the

TABLE V. Parameters used in coupled channels calculations (first-order vibrational model) in fitting elastic, 2_1^+ and 3_1^- data at 22.3 MeV. The other parameters (depths in MeV and geometries in fm) were $r_0=1.165$, $a_0=0.781$, $W=0.5$, $r_w=1.276$, $a_w=0.6+0.85(N-Z)/A$, $V_{so}=6$, $r_{so}=1.01$, $a_{so}=0.75$, $r_C=1.2$.

Nucleus	V_0 (MeV)	W_D(g.s.) (MeV)	$W_D(2^+)$ (MeV)	$W_D(3^-)$ (MeV)	β_2	β_3	$\chi_{0^+}{}^2$	$\chi_{2^+}{}^2$	$\chi_{3^-}{}^2$
^{92}Mo	53.3	8.52	4.21	6.79	0.0645	0.1294	1.58	1.37	1.11
^{94}Mo	53.1	8.30	10.72	7.47	0.1555	0.1496	0.93	1.27	1.50
^{96}Mo	54.1	7.56	11.30	7.81	0.1987	0.1758	1.60	1.14	1.20
^{98}Mo	54.0	8.18	13.36	10.15	0.2080	0.2186	0.78	1.48	1.09
^{100}Mo	54.1	7.84	10.70	10.13	0.2338	0.2118	0.87	1.34	1.76
^{102}Ru	54.1	8.18	11.56	8.72	0.2654	0.1691	0.75	1.06	2.27
^{104}Pd	54.0	7.87	11.61	8.06	0.2342	0.1706	0.52	1.11	1.30
^{106}Pd	53.9	7.73	10.56	8.08	0.2539	0.1639	0.42	0.71	1.96
^{108}Pd	53.9	8.41	11.13	8.18	0.2685	0.1487	0.54	1.06	2.56
^{110}Pd	54.2	8.95	11.20	9.49	0.2736	0.1336	0.56	1.53	3.60
^{106}Cd	52.2	7.62	11.45	8.51	0.1944	0.1705	0.75	1.54	2.99
^{110}Cd	53.8	7.93	11.03	7.24	0.1921	0.1386	0.52	1.01	1.52
^{112}Cd	53.8	8.35	11.52	8.81	0.2006	0.1506	0.40	0.85	1.16
^{116}Cd	54.4	9.51	11.46	9.20	0.2051	0.1288	1.04	1.65	5.00

levels of rotational bands.[28]

Such effects are not found for the transitions to the 3_1^- states. In this case the couplings with multiphonon states seem therefore to play a less important role. The $\beta_3^{pp'}$ obtained are in very good agreement with β_3^{em}. A different situation is found for the quadrupole parameters $\beta_2^{pp'}$, which are strongly dependent both on the coupling scheme and on the choice of $W_D(2_1^+)$. If the coupling with two-phonon states is not considered and the absorption in the elastic and the 2_1^+ channel is fixed in the best fitting procedure, the $\beta_2^{pp'}$ values obtained are larger than β_2^{em} by about 10%. On the other hand, if the constraint $W_D(2_1^+)=W_D$ (g.s.) is imposed, the $\beta_2^{pp'}$ obtained are smaller than β_2^{em} by about 10% and the fits to the 2_1^+ differential cross sections deteriorate significantly. Recently the differences between deformation parameters for the 2_1^+ state extracted from electromagnetic excitation and from hadron scattering have been extensively discussed.[29,30] To evaluate these differences Madsen *et al.*[29] have given a prescription based on the isospin dependence of the effective nucleon-nucleon interaction. It has been usual to discuss the transition

TABLE VI. Parameters used in coupled-channel calculations (second-order vibrational model) in fitting elastic and 2_1^+ data with the coupling scheme (0_0^+-2_1^+-0_2^+-2_2^+-4_2^+). The same imaginary potential has been assumed for all the channels. The other parameters are the same as in Table V.

Nucleus	V_0 (MeV)	W_D (MeV)	β_2	$\chi_{0^+}{}^2$	$\chi_{2^+}{}^2$
^{92}Mo	52.9	8.11	0.0899	1.67	5.50
^{94}Mo	52.5	8.55	0.1424	0.90	1.23
^{96}Mo	53.0	8.03	0.1742	2.23	1.20
^{98}Mo	52.9	8.8	0.1732	0.79	0.80
^{100}Mo	53.0	8.09	0.2211	2.00	1.06
^{102}Ru	52.9	8.10	0.2423	1.44	0.61
^{104}Pd	53.0	8.10	0.2099	1.14	0.80
^{106}Pd	53.1	7.70	0.2268	1.31	0.84
^{108}Pd	53.1	7.91	0.2511	1.60	0.80
^{110}Pd	53.3	8.09	0.2649	1.14	0.57
^{106}Cd	54.2	8.31	0.1714	1.14	1.25
^{110}Cd	53.1	8.28	0.1748	1.10	0.86
^{112}Cd	53.0	8.45	0.1856	1.12	0.73
^{116}Cd	53.4	9.00	0.1884	1.06	1.52

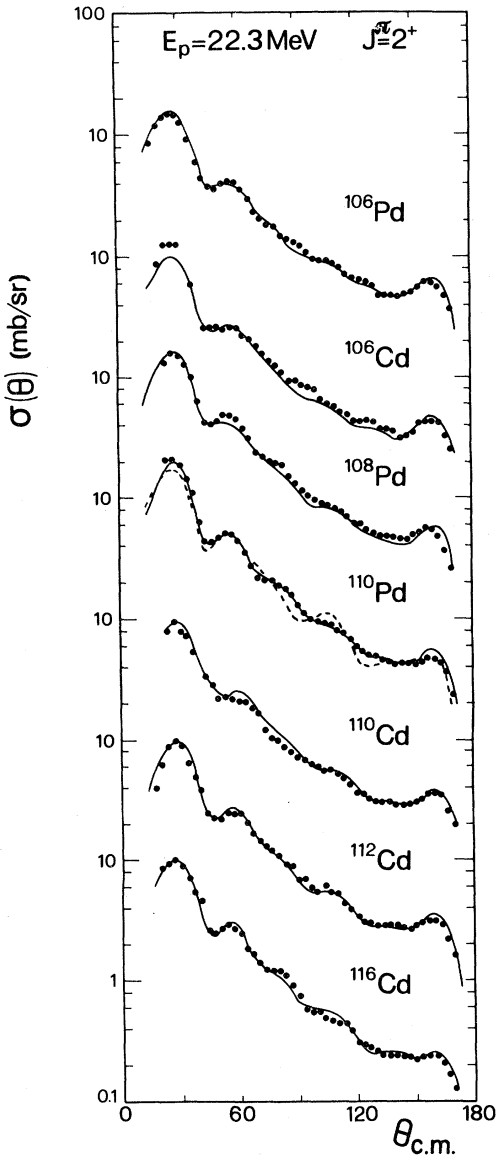

FIG. 11. Same as in Fig. 10, for $106 \leq A \leq 116$ nuclei.

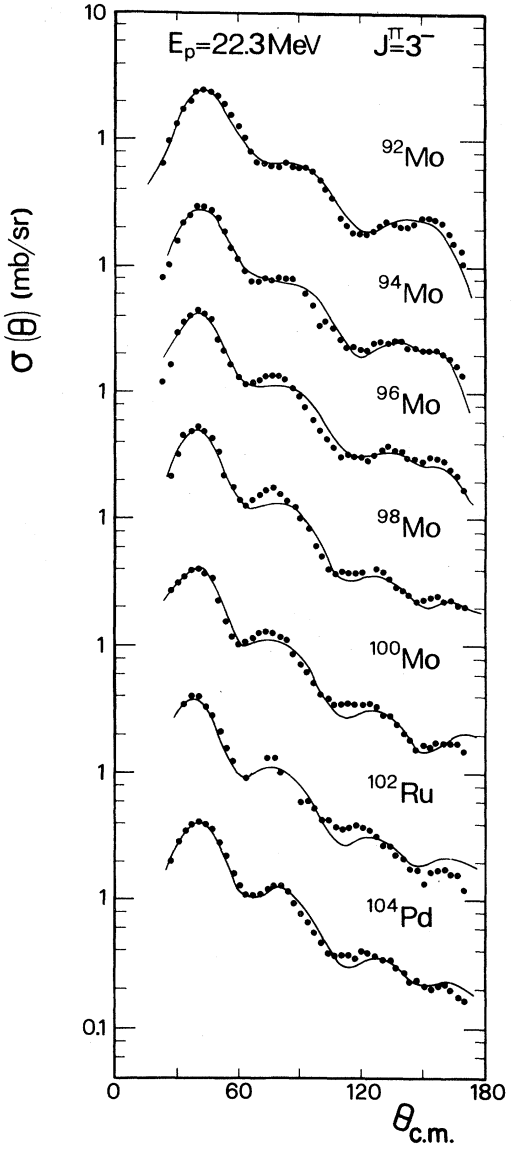

FIG. 12. Differential cross sections for the excitation of the first 3^- state. The solid lines are first-order vibrational model calculations in the coupling scheme $(0_0^+\text{-}2_1^+\text{-}3_1^-)$.

strengths in terms of deformation lengths $\delta=\beta R$, where R is an effective mean OM radius. For proton scattering at low-incident energies, the contributions of the imaginary, spin-orbit, and Coulomb couplings are relatively small so that the form-factor radius can be identified with that of the real term. Moreover, different β values have been used in the present analysis for the different potential terms in order to keep the deformation lengths constant. More recently transition strengths have been compared in terms of multipole moments. For proper comparisons[28] electromagnetic moments $M(E\lambda)^{\text{em}}$, deduced from $B(E\lambda)$ values, are compared with multipole moments from inelastic proton scattering defined as

$$M(E\lambda)^{pp'}=Z\int V(\vec{r})r^\lambda Y_{\lambda 0}(\hat{r})d^3r/\int V(\vec{r})d^3r\ ,$$

where Z is the atomic number of the target and $V(\vec{r})$ is the real part of the deformed OM potential. To stress the dependence of coupling strengths on the assumed couplings, the results obtained from DWBA and CC calculations with $(0_0^+\text{-}2_1^+\text{-}3_1^-)$ and $(0_0^+\text{-}2_1^+\text{-}0_2^+\text{-}2_2^+\text{-}4_2^+)$ schemes are shown in Fig. 14. In these calculations, as in previous similar studies,[29,30] the imaginary potential has been fixed at the same value for all the channels considered. Dif-

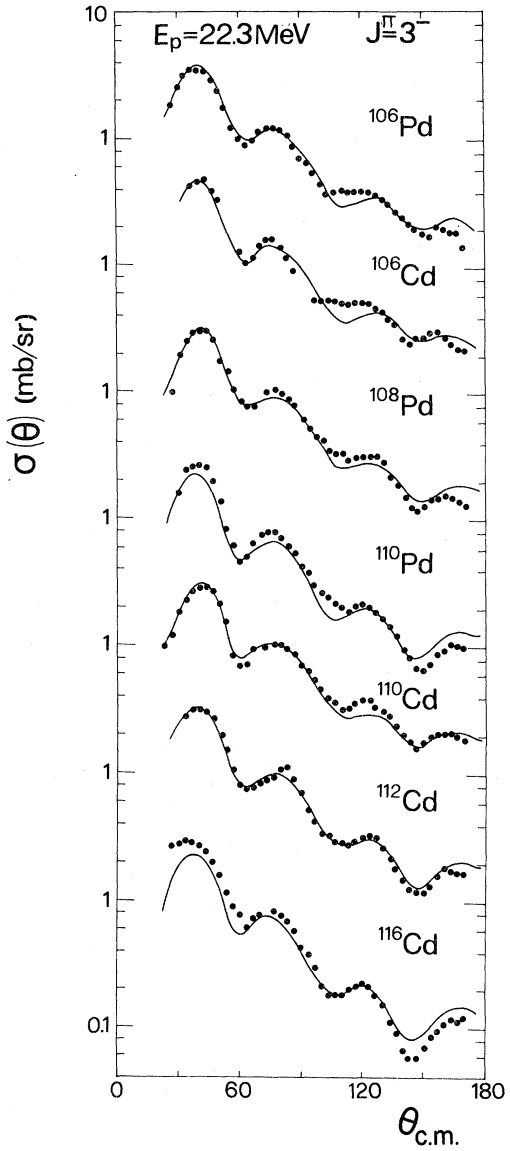

FIG. 13. Same as in Fig. 12.

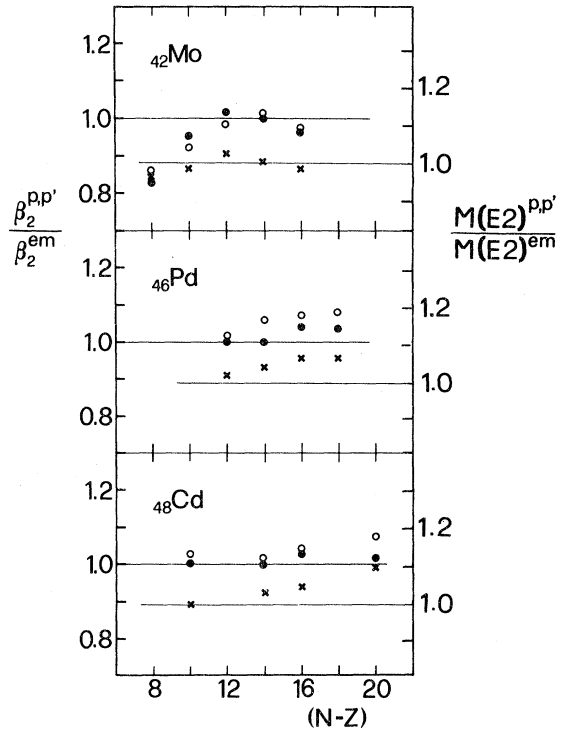

FIG. 14. Ratios of the quadrupole deformation parameters from the present (p,p') experiment to those obtained from Coulomb excitation experiments (left-hand scale). The $\beta_2^{pp'}$ values have been obtained from DWBA analyses (empty points) and from coupled-channel calculations with the coupling scheme $(0_0^+\text{-}2_1^+\text{-}3_1^-)$ (crosses) and with the coupling scheme $(0_0^+\text{-}2_1^+\text{-}0_2^+\text{-}2_2^+\text{-}4_2^+)$ (full points). The right-hand scale gives the ratios of the quadrupole moments.

ferent coupling schemes can account for differences in $\beta_2^{pp'}$ values of the order of 10%. Very similar $\beta_2^{pp'}$ and β_2^{em} values are found using the second scheme, in agreement with the findings of the recent survey by Matoba.[30] The corresponding $M(E2)^{pp'}/M(E2)^{em}$ ratio is larger than one since the rms radii of the OM potentials are larger than those of electric charge distributions. A better agreement in the quadrupole moments is obtained when both 2_1^+ and 3_1^- channels are taken into account as shown in Fig. 14 for the $(0_0^+\text{-}2_1^+\text{-}3_1^-)$ coupling. Similar results are obtained with the $(0_0^+\text{-}2_1^+\text{-}3_1^-\text{-}0_2^+\text{-}2_2^+\text{-}4_2^+)$ coupling (see Table IV). The relatively small $R\beta 2$ value found in the case of ^{92}Mo can be compared with the predictions of the schematic model of Madsen *et al.*[29] for single closed shell nuclei (see the next section).

Finally it should be noted (Fig. 8) that the discrepancy in the asymmetry dependence of V_0, found in OM calculations, is strongly reduced with the $(0_0^+\text{-}2_1^+\text{-}0_2^+\text{-}2_2^+\text{-}4_2^+)$ scheme and completely absent with the $(0_0^+\text{-}2_1^+\text{-}3_1^-)$ scheme.

The main conclusion of the comparisons described in this section (which is in fact rather obvious, but surprisingly often overlooked) is that in an extended OM calculation the crucial point lays in the choice of the collective couplings between channels. The elastic channel can be described by completely standard OM parameters if the couplings with the relevant one-phonon states are properly considered. Similarly the differential cross sections for the 2_1^+ channel are well described, with transition strengths in agreement with the electromagnetic values and with standard OM parame-

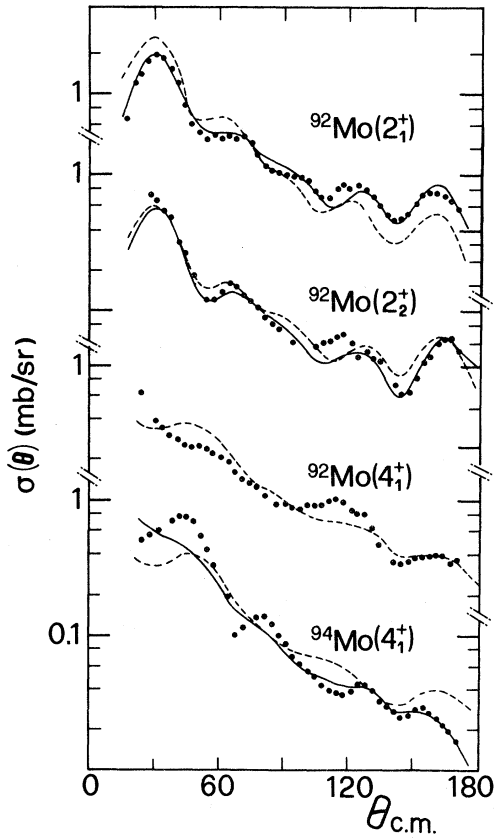

FIG. 15. Experimental differential cross sections and coupled channels calculations: (1) ^{92}Mo(2_1^+), best fits with W_D(g.s.)$=W_D(2_1^+)$ (dashed curve) and with W_D(g.s.) and $W_D(2_1^+)$ fixed independently (solid curve); (2) ^{92}Mo(2_2^+), one-phonon excitation with $\beta''_{02}=-0.036$ (dashed curve), one- plus two-phonon excitation with $\beta''_{02}=-0.033$ and $\beta_{22}=-0.07$ (solid curve); (3) ^{92}Mo(4_1^+) one-phonon excitation with $\beta''_{04}=0.05$; (4) ^{94}Mo(4_1^+), one-phonon excitation with $\beta''_{04}=0.092$ (dashed curve), one- plus two-phonon excitation with $\beta''_{04}=0.07$ and $\beta_{24}=-0.207$ (solid curve). For the meaning of β's symbols see Fig. 16.

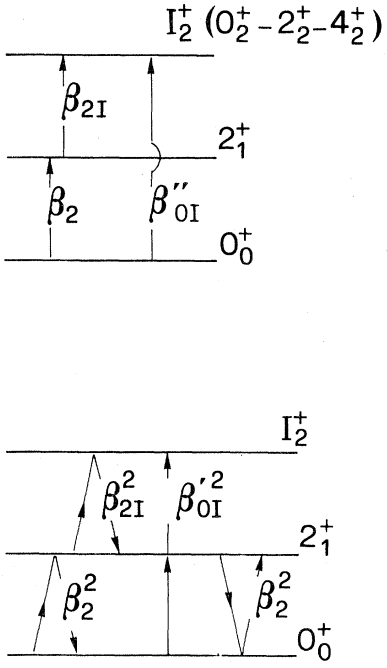

FIG. 16. Schematic representation of the coupling strengths in the vibrational model. First-order terms arising from quadrupole-phonon excitations are shown in the upper part, terms representing the relevant second-order transitions in the lower part.

ters, if the couplings with two-phonon states are considered.

B. ^{92}Mo data analysis

The analysis of the ^{92}Mo data must be discussed separately from the other isotopes because of their distinctive features. The average angular slope of the differential cross sections for the 2_1^+ state is less steep than that for the other nuclei and the oscillations in the median angular region are more pronounced. Similar features are present, although less evident, for the transition to the 3_1^- state. Because of these features no coupling of the 2_1^+ with other channels is required and the $\beta_2^{pp'}$ and $W_D(2_1^+)$ found are much smaller than β_2^{em} and W_D (g.s.), respectively; the obtained ratio $R\beta 2$ of 0.6 is lower than that for the other nuclei considered here. The reliability of this result is, however, limited by the very low value used for $W_D(2_1^+)$ (about half of that for the g.s.) and by the well-known ambiguity[4] between $\beta_2^{pp'}$ and $W_D(2_1^+)$ values. The dashed curve shown in Fig. 15 for the 2_1^+ transition has been obtained with $W_D(2_1^+)=W_D$ (g.s.); its average angular dependence is too steep, while the ratio of β_2 values is 0.64, when calculations are normalized at forward angles, and 0.83 with the best-fit normalization shown in the figure. These values of the ratio $R\beta 2$ are in reasonable agreement with the model of Madsen[29] which predicts for a proton transition in ^{92}Mo a ratio of 0.65. The structure of the low-lying states of this nucleus should be in fact mainly due to the excitation of the two protons outside of the doubly magic core of ^{90}Zr. The differential cross sections for the other inelastic transitions in ^{92}Mo can be described, at least approximately, as simple one-phonon excitations, while already for ^{94}Mo, as shown in Fig. 15 in the case of the transition to the first 4^+ excited state, the need for more complex couplings is evident.

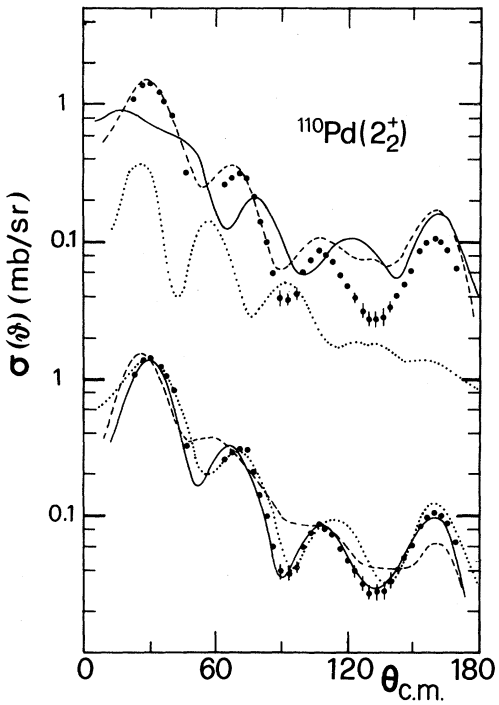

FIG. 17. Typical results for 2_2^+ cross sections obtained in the framework of harmonic and anharmonic vibrational models. Upper part: contribution of the two-step $(0_0^+\text{-}2_1^+\text{-}2_2^+)$ term alone with $\beta_{22}=\beta_2$ (dashed curve), second-order contribution with $\beta'^2_{02}=\beta_2\cdot\beta_{22}=\beta_2^2$ (dotted curve); the solid curve is the sum of these two contributions. Lower part: anharmonic vibrator model with pure one-phonon excitation and $\beta''_{02}=0.07$ (dashed curve), with one- plus two-phonon excitation and $\beta''_{02}=0.066$, $\beta_{22}=\beta_2$, $\beta'^2_{02}=\alpha\beta_2^2$ where $\alpha=[1-(\beta'_{02}/\beta_2)^2]^{1/2}$ (dotted curve) and with $\beta''_{02}=0.033$, $\beta_{22}=0.151$, and $\beta'_{02}=0$, i.e., without second-order terms (solid curve).

C. Two-quadrupole-phonon states and the anharmonic vibrator model

The coupling scheme currently used for the analysis of the transitions leading to the second 0^+ and 2^+ states and to the first 4^+ excited state in the Mo-Ru-Pd-Cd region is displayed in Fig. 16. In an ideal harmonic vibrator model, these states should be located at the same excitation energy, which should be twice as large as that of the 2_1^+ state. In the same model the reduced matrix elements to be used in CC calculations can be evaluated[12] from a single β_2 value since β_{2I} is assumed equal to β_2. In second-order calculations the transitions, such as $(0_0^+\text{-}2_1^+\text{-}0_0^+,\ L=0)$, $(2_1^+\rightarrow 0_0^+\rightarrow 2_1^+,\ L=0,2,4)$, $(0_0^+\rightarrow 2_1^+\rightarrow I_2^+,\ L=I)$, etc., are also considered. The strengths of all these transitions are quadratic in β_2; the last one, β'^2_{0I}, is taken equal to $\beta_2\cdot\beta_{2I}$ and is therefore also proportional to β_2^2. The transition densities of the first- and second-order couplings are taken, respectively, as the first and second derivatives of the OM form factors.

This coupling scheme has been used in a preliminary analysis and does not imply that the 0_2^+, 2_2^+, and 4_2^+ states can be treated as pure two-quadrupole-phonon states. In all cases the transitions to the 2_2^+ and 4_2^+ states are in fact better described by adding significant single-phonon components with coupling strengths β''_{0I} to the ground state. However, this kind of analysis gives values of β in definite disagreement with Coulomb-excitation data (CE). As was shown by Robinson *et al.*,[4] for several Pd and Cd isotopes, one finds $(\beta''_{02})^{pp'}/(\beta''_{02})^{CE}=2$, $(\beta_{2I})^{pp'}/(\beta_{2I})^{CE}=0.4-0.8$, and therefore a smaller second-order amplitude β'^2_{0I}, since these last coupling strengths are proportional to $\beta_2\cdot\beta_{2I}$. These results can be understood by looking at the various contributions to the excitation of the triplet states. In Fig. 17 the results for the 2_2^+ state of ^{110}Pd are shown. The contribution coming from the two-step term of the coupling $(0_0^+\text{-}2_1^+\text{-}2_2^+)$ gives a calculated angular distribution with a diffraction pattern which is in phase with the experiment, while the second-order term $(0_0^+\text{-}2_1^+\text{-}2_2^+)$ is completely out of phase. When this last term is coherently summed with the first term an angular distribution is obtained which is still in marked disagreement with the experiment. To reduce the disagreement, the amplitude of this second-order contribution, i.e., the value of β'^2_{02} and therefore that of β_{22} was reduced by a factor 2, while the amplitude β''_{02} of the first-order one-phonon coupling between the 2_2^+ and ground state was increased. In the lower part of Fig. 17 it is shown that by neglecting the β'^2_{02} amplitude (as in first-order calculations) it is possible to obtain more satisfactory fits with a value of β''_{02} which is lower and in better agreement with the results of Coulomb-excitation experiments.

The failures of earlier analyses of two-phonon transitions may therefore be connected with the assumptions made for the second-order terms. Similar results were also obtained in the case of 4^+ states. Relatively few experiments and analyses have been reported for 0_2^+ states[3]; consequently, for these transitions, definite conclusions are not possible. Considering these difficulties it is quite evident why new CC calculations based on a different approach are of some importance for the understanding of the excitation mechanism of these two-phonon states.

V. IBA MODEL AND CC CALCULATIONS

The Mo, Ru, Pd, and Cd isotopes span a transition region from nuclei exhibiting single-particle properties (^{92}Mo) to nuclei with vibrator properties and more or less pronounced anharmonicity. Moreover, the features of some of their excited states are connected to permanent deformations. A theoretical approach appropriate for describing transitional regions is provided by the IBA model. In this model nucleon pairs are represented in terms of N bosons outside closed shells. Descriptions have been given[8-11,31-33] in which the bosons are allowed to occupy two levels: the ground-state level with angular momentum $L=0$ (s boson) and an excited one with $L=2$ (d boson). The model space can be expanded to include other pairs, such as f bosons ($L=3$) and g bosons ($L=4$). It is possible to calculate within the chosen space several nuclear properties by specifying the appropriate operators and wave functions. A description of the general form of these transition operators is given in Refs. 9 and 10. With the calculated pairs limited to s and d bosons, one obtains the following transition densities:

$$E0:\ \rho_{0_i^+\to 0_j^+}(r)=[\rho_{\text{core}}+\alpha_0(r)N]\delta_{ij}+\beta_0(r)B_{ij}^{(0)}\ ,$$

$$E2:\ \rho_{0_i^+\to 2_j^+}(r)=e^{(2)}[\alpha_2(r)A_{ij}^{(2)}+\beta_2(r)B_{ij}^{(2)}]\ ,$$

$$E4:\ \rho_{0_i^+\to 4_j^+}(r)=e^{(4)}\beta_4(r)B_{ij}^{(4)}\ .$$

These transition densities describe the coupling of the pairs to the external electromagnetic or nuclear fields. The weighting factors $e^{(\lambda)}$ must be connected to some effective interaction. In electron scattering they are replaced by effective charges. In proton scattering we use simply the strengths of the different OM potential terms. The matrix elements $B_{ij}^{(\lambda)}$ are given, respectively, by

$$B_{ij}^{(0)}=\langle 0_j^+||(d^\dagger d)^{(0)}||0_i^+\rangle\ ,$$

$$A_{ij}^{(2)}=\langle 2_j^+||(d^\dagger s+s^\dagger d)||0_i^+\rangle\ ,$$

$$B_{ij}^{(2)}=\langle 2_j^+||(d^\dagger d)^{(2)}||0_i^+\rangle\ ,$$

$$B_{ij}^{(4)}=\langle 4_j^+||(d^\dagger d)^{(4)}||0_i^+\rangle\ ,$$

and were calculated using the IBA-2 Hamiltonian.[31-33] In analyses considering only static properties, the coupling factors $\alpha_2(r)$ and $\beta_\lambda(r)$ were taken as numbers. In studying scattering processes these numbers must be replaced by form factors describing the spatial dependence of the coupling. This dependence is connected to the single-particle densities and, in principle, can be obtained from a shell model calculation. In a less ambitious approach the above form factors are deduced empirically from the analysis of scattering experiments. The quadrupole densities $\alpha_2(r)$ and $\beta_2(r)$ have been extracted from the analysis of electron scattering on some medium-heavy nuclei (^{150}Nd and samarium isotopes[10,11]). The form factor $\alpha_2(r)$ is surface peaked and sufficiently well reproduced by the first derivative of a Woods-Saxon distribution, while $\beta_2(r)$ displays a node at a radial distance somewhat smaller than the nuclear radius and can be approximated by a second derivative of a Woods-Saxon potential with a radius reduced with respect to that used for $\alpha_2(r)$ by a factor varying from 0.87 (^{150}Nd) to 0.6 (Sm isotopes). Here one could mention that these form factors have been obtained for a region of deformed nuclei and that slight differences might arise in the Pd region. No reliable information has been obtained for $\beta_0(r)$ and $\beta_4(r)$.

The spectroscopic amplitudes B_{ij}, used in the present (pp') calculations, already include appropriate weighting factors (χ_ν and χ_π of Refs. 31-33). At least for the quadrupole transitions, these should ensure the correct phase and amplitude, as needed by $B(E2)$ data, for the $(d^\dagger d)^{(2)}$ contributions. The ratio of the quadrupole moments

$$\int\beta_2(r)r^2d^3r/\int\alpha_2(r)r^2d^3r$$

(which was taken equal to -1.5 in the analysis of Ref. 11) should therefore be equal to 1.

In our case the diagonal term $[\rho_{\text{core}}+\alpha_0(r)N]$ is replaced by the OM potential and the $\alpha_2(r)$ form factor is obtained from the first derivative of the same potential. This last sample prescription gives generally satisfactory results.

Less straightforward is the choice of the $\beta_\lambda(r)$ radial dependence, also because these form factors are connected with the $(d^\dagger d)^{(\lambda)}$ transition amplitudes, which are generally smaller than the $(d^\dagger s+s^\dagger d)^{(2)}$ amplitudes. However, for the $\beta_2(r)$ form factor some information has been obtained from the analysis of 2_2^+ data. The $(d^\dagger d)^{(2)}$ amplitude is in fact relatively large in the coupling $(0_0^+\text{-}2_2^+)$ and is also present in the coupling $(2_1^+\text{-}2_2^+)$. No attempts have been made to differentiate between the $\beta_2(r)$ form factors to be used for these and the other quadrupole couplings. The best fits to the 2_2^+ angular distributions have been obtained assuming a second derivative of the OM potential and by adjusting the form factor radius. To reduce the ambiguities of the best-fitting procedure, the variation in the radii of the different potential terms (real, imaginary, spin-orbit, and Coulomb) is constrained to keep the relative values unchanged. Moreover the potential strengths are renormalized so as to keep

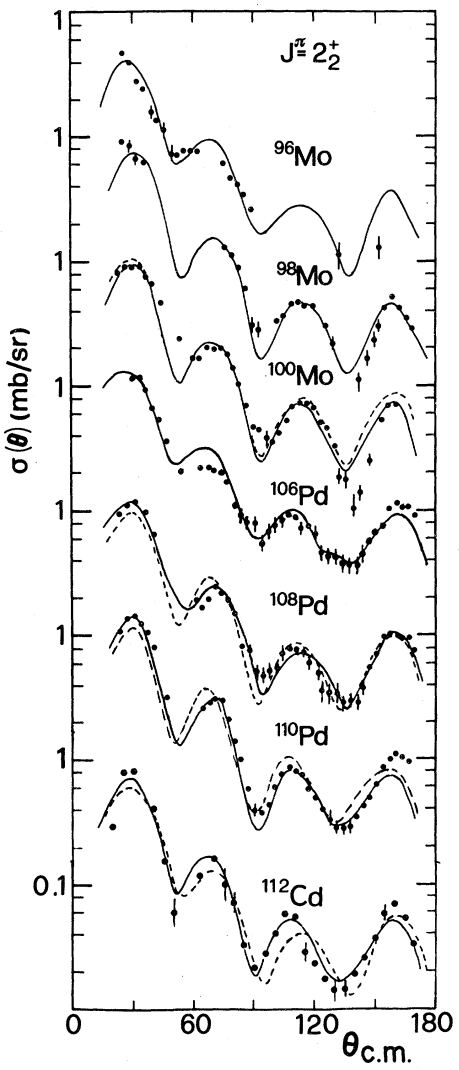

FIG. 18. Differential cross sections for transitions leading to 2_2^+ states and CC predictions obtained with spectroscopic amplitudes derived from the IBA model (in the case of ^{106}Pd to the 2_2^+ and 0_2^+ states, which were not resolved). The solid curves have been obtained using a form factor $\beta_2(r)$ (see text) given by a second derivative of the OM potential with a radius reduced by factors of 0.91 (^{96}Mo), 0.92, (^{98}Mo), 0.97 (^{100}Mo), 0.85, (^{106}Pd), 0.98 (^{108}Pd), 0.95 (^{110}Pd), and 0.85 (^{112}Cd). Dashed curves are the results obtained without reduction of the radius (^{100}Mo and ^{112}Cd) or using a first derivative (^{108,110}Pd).

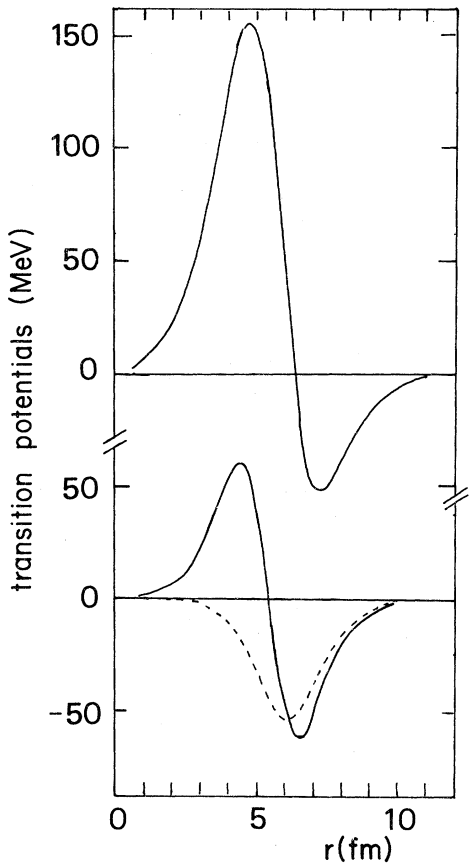

FIG. 19. Real part of the transition form factors used in CC calculations with IBA spectroscopic amplitudes. Upper part: $\beta_0(r)$ monopole form factor from surface oscillations used in ^{116}Cd(0_2^+) calculations. In the lower part the solid and dashed curves give, respectively, the quadrupole $\beta_2(r)$ form factor used to obtain the solid and dashed curves of Fig. 18 for ^{108}Pd(2_2^+) data.

the above ratio of radial quadrupole moments equal to one. The best-fit radius is slightly reduced in comparison to the OM potential radius. The reduction required by the different nuclei varies between 2–3% (^{100}Mo, ^{108}Pd) and about 15% (^{106}Pd, ^{112}Cd). Since this is the only parameter searched on in the fits to the 2_2^+ data, any shortcoming of the IBA model or of the CC calculations can affect the best-fit value and makes it difficult to connect these differences to nuclear structure properties, however, the presence of a node slightly inside the nuclear surface in the $\beta_2(r)$ form factor is well established.

For the purpose of comparison, the cross sections obtained without a reduction of the radius of the $\beta_2(r)$ form factor are shown in Fig. 18 for ^{100}Mo and ^{112}Cd. Also less satisfactory, but still acceptable (dashed curves on ^{108}Pd and ^{110}Pd) are the fits obtained using a first derivative with a radius slightly larger than the OM radius. This result can be understood considering the similarity of the two form factors in the surface region, as shown by the graphs of Fig. 19. This means that the proton scattering is less affected by the inner part of the transition form factor.

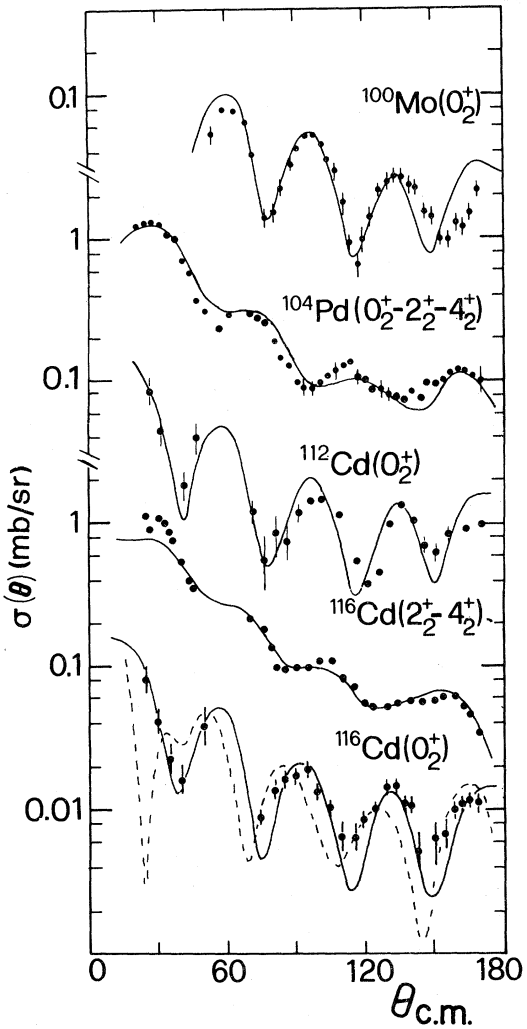

FIG. 20. Comparisons between experimental cross sections and CC calculations with IBA amplitudes (solid curves). The dashed curve for the 0_2^+ transition on ^{116}Cd shows the effect of changing the sign of the $\beta_2(r)$ transition density.

In the cases of ^{96}Mo and ^{98}Mo the curves of Fig. 18 are normalized by factors of 16 and 1.5, respectively. A large failure of the IBA calculations has been found also in the comparison with the $B(E2)$ values.[32] This discrepancy is probably due to the small number of nucleons outside the ^{90}Zr core. However, even in this case, the calculation predicts correct $B(E2)$ ratios and, in our case, a correct mixture of the different contributions to the excitation of the 2_2^+ state. This is supported by the good agreement in the shape of the angular distributions. The 2_2^+ transitions in ^{100}Mo, ^{106,108,110}Pd, and ^{112}Cd are reproduced also in magnitude.

The IBA calculations give correct predictions (Fig. 20) also for ^{104}Pd and ^{116}Cd, where the states

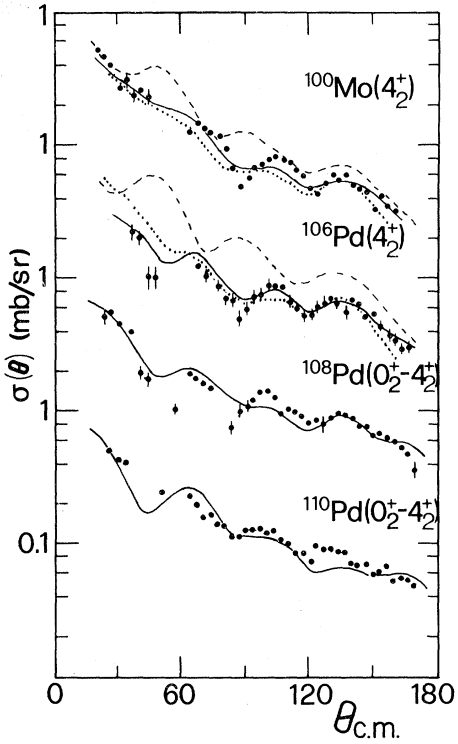

FIG. 21. The same as in Fig. 18 for transitions to 4^+ states. The different curves have been obtained with different prescriptions for the $\beta_4(r)$ form factors: (a) using the second derivative (solid curves); (b) using the first derivative (dotted curves on ^{100}Mo and ^{106}Pd data); (c) using the second derivative and the opposite phase (dashed curves).

of the triplet (0_2^+-2_2^+-4_2^+) are not resolved. In the same figure are also shown the differential cross sections for the excitation of the 0_2^+ state in ^{100}Mo, ^{112}Cd, and ^{116}Cd. The agreement between experimental and calculated angular distributions, obtained without any normalization, can be considered very satisfactory in view of the difficulties usually found in fitting monopole transitions. The comparison with the experiment could give some indication on the $\beta_0(r)$ form factor. It should, however, be noted that the monopole (0_1^+-0_2^+) contribution to the 0_2^+ cross section is predominant only at forward angles, while the two-step (0_0^+-2_1^+-0_2^+) contribution is dominant over the rest of the angular range.

As a first trial one can assume for $\beta_0(r)$ a second derivative as for $\beta_4(r)$. However, also leaving the radius free to vary, no satisfactory results have been obtained. Following Ref. 10 $\beta_0(r)$ should be given by a linear combination of terms expressed by first and second derivatives. The resulting sum is very similar to the form factor predicted for a vibration in the surface thickness (radius and diffuseness oscillations[34]). This last form factor can be given as

$$\beta_0(r) = -KZR\frac{dU(r)}{dr}[(1+Z)/Z - r/R] ,$$

where $U(r)$ is the optical model potential, R the potential radius, $Z=(3+y^2)/2y^2$ (with $y=\pi a/R$) for a volume Woods-Saxon term, and $2/(1+y^2)$ for a surface term given by the first derivative of a Woods-Saxon. The normalization constant K resulting from the best fit of the 0_2^+ angular distributions is 1.2 ± 0.2. The solid curves on ^{100}Mo, ^{112}Cd, and ^{116}Cd data in Fig. 20 have been deduced with this latter form factor. The same prescription has been used for all the other $L=0$ couplings, which are present in recoupling transitions ($J_i \rightarrow J_i$) and in the transition ($2_1^+ \rightarrow 2_2^+$).

Our data for 4^+ transitions are shown in Fig. 21. The IBA calculations reproduce the cross-section magnitudes and the shape of the angular distributions over the full angular range. The most satisfactory fits have been obtained taking the radial dependence of $\beta_4(r)$ as the second derivative of the OM potential:

$$\beta_2(r) = -\frac{KR^2}{2}\frac{d^2U(r)}{dr^2} ,$$

where the potential radius was generally reduced by a very small amount (2–3 %). The tests of $\beta_4(r)$ geometries have been performed keeping a constant value for the hexadecapole radial moment

$$M(E4)^{pp'} = \int \beta_4(r) r^4 d^3r .$$

The normalization constant K obtained for these transitions is equal to about 0.5 for all nuclei. This normalization together with a reduction of 2.5% of the radius gives a radial moment of the same value as that obtained using a first derivative form factor, that is,

$$\beta_4(r) = -R\frac{dU(r)}{dr} .$$

To show the influence on $L=4$ transitions of the radial dependence of $\beta_4(r)$, the results obtained using the first derivative are also shown in Fig. 21 (dotted curves for ^{100}Mo and ^{106}Pd).

The calculated cross sections for 0_2^+ and 4_2^+ transitions are strongly affected by the phase of the transition density, as shown in Figs. 20 and 21. As a general rule, for the nuclei considered here, the transition densities for $(0_1^+\text{-}I_2^+)$, where I_2^+ stands for 0_2^+, 2_2^+, or 4_2^+, should have the same sign as that of the product of the densities for the transitions $(0_0^+\text{-}2_1^+)$ and $(2_1^+\text{-}I_2^+)$. This is obtained for all the nuclei considered here taking K as positive in the above formulae.

VI. CONCLUSIONS

The OM parameters obtained in the present analysis of proton elastic scattering differential cross sections on mass-100 nuclei evidence two distinct nuclear structure effects: an anomalous isospin dependence of the real well depth for Pd and Cd isotopes and imaginary terms for Pd, Cd, and the heavier Mo isotopes which are 20% larger than those of average phenomenological optical potentials.[26] Both effects can be explained in terms of collective couplings with the low-lying one-phonon states. Structure effects concerning the magnitude of the imaginary terms were already revealed, in the case of lighter nuclei,[35] in the correlation existing between the total reaction cross sections, the imaginary terms in the OM potentials, and the deformation parameters for the ground-state rotational or vibrational bands.

Arguments and numerical evaluations are given in Sec. III to show that the anomalously large values of the imaginary terms found in OM analyses at sub-Coulomb energies can be practically eliminated if these are performed with more flexibility in the choice of the geometrical parameters. No evidence has been found in any case of similar anomalies at higher incident energies.

The 2_1^+ and 3_1^- one-phonon channels are satisfactorily reproduced by collective vibrational model calculations with transition moments in agreement, within a few percent, with those deduced from Coulomb excitation experiments. This result, in the case of the 2_1^+ channel, is, however, obtained only when other couplings, and in particular that to the first octupole state, are taken into account. The differential cross sections for the transitions leading to two-quadrupole-phonon states are less satisfactorily reproduced by collective macroscopic models. In this study we show that these transitions can instead be accounted for by coupled channels calculations using spectroscopic amplitudes obtained from the interacting boson approximation. The form factors are derived with simple prescriptions from OM potentials. The usual first derivative gives the form factor for $(s^\dagger d + d^\dagger s)^{(2)}$ transitions and gives also acceptable form factors for the $(d^\dagger d)^{(\lambda)}$ transitions. The quadrupole $(d^\dagger d)^{(2)}$ transitions are, however, better reproduced by a second derivative with a radius reduced, in comparison to the OM potential radius, by a factor of 0.85–0.97. This result is similar to that deduced from the analysis of electron scattering experiments. The

best-fit reduced radii are the result of a search in which the radial moment

$$M(E2)^{pp'}=\int \beta_2(r) r^2 d^3r$$

was kept constant by adjusting the potential strength. A variation of this moment, which corresponds to the $B(E2)$ value, is in fact equivalent to a modification of the IBA spectroscopic amplitudes.

The 0_2^+ transitions are satisfactorily reproduced taking a monopole form factor with the radial dependence predicted for surface oscillations. Further work is in our opinion necessary to determine more precisely the hexadecapole form factor, also because the 4^+ transitions might be affected by the inclusion of the g boson.

[1]C. H. Johnson, A. Galonsky, and R. L. Kernell, Phys. Rev. C 20, 2052 (1979).

[2]R. L. Robinson, J. L. C. Ford, Jr., P. H. Stelson, and G. R. Satchler, Phys. Rev. 146, 816 (1966).

[3]H. F. Lutz, W. Bartolini, and T. H. Curtis, Phys. Rev. 178, 1911 (1969).

[4]R. L. Robinson, J. L. C. Ford, Jr., P. H. Stelson, T. Tamura, and C. Y. Wong, Phys. Rev. 187, 1609 (1969).

[5]M. Koike, I. Nonaka, J. Kokame, H. Kamitsubo, Y. Awaya, T. Wada, and H. Nakamura, Nucl. Phys. A125, 161 (1969).

[6]H. F. Lutz, D. W. Heikkenen, and W. Bartolini, Phys. Rev. C 4, 934 (1971).

[7]M. Koike, T. Suehiro, K. Pingel, K. Komura, I. Nonaka, T. Wada, T. Fujisawa, H. Kamitsubo, and T. Nojiri, Nucl. Phys. A248, 237 (1975).

[8]T. Kishimoto and T. Tamura, Nucl. Phys. A192 264 (1972); K. Weeks and T. Tamura, Phys. Rev. C 22, 888 (1980).

[9]A. Arima, T. Otsuka, F. Iachello, and I. Talmi, Phys. Lett. 66B, 205 (1977).

[10]F. Iachello, Nucl. Phys. A358, 89 (1981).

[11]A. E. L. Dieperink, F. Iachello, A. Rinat, and C. Creswell, Phys. Lett. 76B, 135 (1978); M. A. Moinester, G. Azuelos, J. Alster, and A. E. L. Dieperink, Nucl. Phys. A383, 264 (1982).

[12]T. Tamura, Rev. Mod. Phys. 37, 679 (1965).

[13]ECIS coupled channel computer code by J. Raynal.

[14]F. K. McGowan, R. L. Robinson, P. H. Stelson, and J. L. C. Ford, Nucl. Phys. 66, 97 (1965).

[15]R. L. Robinson, F. K. McGowan, P. H. Stelson, W. T. Milner, and R. O. Sayer, Nucl. Phys. A124, 553 (1969).

[16]J. Barrette, M. Barrette, A. Boutard, R. Haroutunian, G. Lamoureux, and S. Monaro, Phys. Rev. C 6, 1339 (1972).

[17]P. Paradis, G. Lamoureux, R. Lecomte, and S. Monaro, Phys. Rev. C 14, 835 (1976).

[18]M. T. Esat, D. C. Kean, R. H. Spear, and A. M. Baxter, Nucl. Phys. A274, 237 (1976).

[19]S. Landsberger, R. Lecomte, P. Paradis, and S. Monaro, Phys. Rev. C 21, 588 (1980).

[20]P. H. Stelson and L. Grodzins, Nucl. Data 1, 21 (1965).

[21]S. Raman, W. T. Milner, C. W. Nestor, Jr., and P. H. Stelson, in *Proceedings of the International Conference of Nuclear Structure, Tokyo, 1977,* edited by T. Marumori (Physical Society of Japan, Tokyo, 1978), p. 79; and private communication.

[22]M. Maynard, D. C. Palmer, J. R. Cresswell, P. D. Forsyth, I. Hall, and D. G. E. Martin, J. Phys. G 3, 1735 (1977).

[23]A. E. Antropov, T. Baiyumi, V. P. Gusev, P. P. Zarubin, P. D. Ioannu, and B. N. Orlov, Yad. Fiz. 29, 1432 (1979) [Sov. J. Nucl. Phys. 29, 734 (1979)].

[24]I. Angeli and M. Csatlos, Nucl. Phys. A288, 480 (1977).

[25]R. Schrils, D. S. Flynn, R. L. Hershberger, and F. Gabbard, Phys. Rev. C 20, 1706 (1979).

[26]F. D. Becchetti and G. W. Greenlees, Phys. Rev. 182, 1190 (1969).

[27]J. R. Comfort, Phys. Rev. Lett. 42, 30 (1979).

[28]L. F. Hansen, I. D. Proctor, D. W. Heikkinen, and V. A. Madsen, Phys. Rev. C 25, 189 (1982); M. M. Gazzaly *et al., ibid.* 25, 408 (1982).

[29]V. A. Madsen, V. R. Brown, and J. S. Anderson, Phys. Rev. C 12, 1205 (1975).

[30]M. Matoba, Phys. Lett. 88B, 249 (1979).

[31]P. Van Isacker and G. Puddu, Nucl. Phys. A348, 125 (1980).

[32]M. Sambataro and G. Molnár, Nucl. Phys. A376, 201 (1982).

[33]M. Sambataro, Nucl. Phys. A380, 365 (1982).

[34]G. R. Satchler, Nucl. Phys. A100, 481 (1967).

[35]E. Fabrici, S. Micheletti, M. Pignanelli, F. Resmini, R. De Leo, G. D'Erasmo, and A. Pantaleo, Phys. Rev. C 21, 844 (1980).